In Vitro and *in Vivo* Metabolism of the Anti-Cancer Agent CI-1040, a MEK Inhibitor, in Rat, Monkey, and Human

Paul A. Wabnitz,[1,4] David Mitchell,[2] and David A.M. Wabnitz[3]

Received March 2, 2004; accepted May 16, 2004

Purpose. The use of *in vitro* and *in vivo* models using both rodent and non-rodent species plays an important role with regard to metabolism during the drug development process. In this study, we compared the metabolism of a MEK inhibitor (CI-1040) using *in vitro* and *in vivo* models with that observed in a cancer patient.

Methods. Radiolabeled CI-1040 was assessed for metabolism using rat and monkey liver microsomes and hepatocytes, as well as in Wistar rats and cynomolgus monkeys via oral administration. Human bile and plasma samples were obtained immediately after administration of CI-1040 to a patient with advanced colon cancer. A combination of HPLC-radiochromatography (HPLC-RAM), LC/MS and LC/MS/MS experiments were used to analyze all resulting metabolites. Unlabeled CI-1040 was administered (100 mg/day, QD) for 15 days to a patient suffering from colon cancer. Bile was collected by the insertion of a T-tube directly into the bile duct over a 14-h period. Metabolites were also monitored in the patient's plasma.

Results. Analysis of the metabolites in all species using *in* vitro and animal models demonstrated that CI-1040 undergoes extensive oxidative metabolism (14 metabolites identified) with subsequent glucuronidation of the hydroxylated metabolites. Metabolites were predominantly excreted through the bile in the animal models.

Conclusions. Overall, the *in vitro* and animal models in combination provided comprehensive coverage for all metabolites observed in human bile and plasma. In conclusion, the results obtained in this study demonstrate the utility of conducting investigations across species in order to gain complete coverage for successfully predicting human metabolites of new compounds in development.

KEY WORDS: cross species comparison; human bile; LC-MS; LC-MSMS; mass spectrometry; MEK; metabolism; oncology.

INTRODUCTION

Approximately 3.2 million people are diagnosed with cancer annually in the United States, Europe, and Japan (1). Of these, some 1.4 million are unresponsive to current therapy. The medical need for oncology therapy therefore continues to remain high, as cancer still remains the second leading cause of death in the Western world, exceeded only by cardiovascular disease (2). Of the current drugs targeting various cancers, MAP-Erk Kinase (MEK) inhibitors are atypical in selectively inhibiting various signals in the mitogenic cascade (3–7). MEK is involved in the transmission of oncogenic and proto-oncogenic signals (3, 8-10). Therefore, a substance that blocks these key-signaling molecules that are involved in tumor growth, progression and metastasis, would be of significance in the treatment of cancer, and inflammatory diseases. MEK plays an integral role in the Ras-Raf-MEK-Erk pathway (Fig. 1), an important mitogenesis signal transduction route in tumors (11-19). This is evident by cell lines derived from pancreas, colon, lung, ovary, breast and kidney tumors displaying particularly high-level expressions of activated Erk (20–21). Therefore, MEK inhibitors suppress the transmission of oncogenic and proto-oncogenic signals to the nucleus indicating the potential effectiveness of MEK as a general target for therapy, compared with other agents that only block one portion of the tumor's highly redundant proliferative pathway (15,22).

CI-1040 (2-(2-chloro-4-iodo-phenylamino)-N-cyclopropylmethoxy-3, 4-difluoro-benzamide, Fig. 2) is a potent and highly selective inhibitor of MEK. CI-1040 directly inhibits purified MEK with a 50% inhibitory concentration (IC_{50}) of 17 nM (23). This inhibition prevents the phosphorylation of Erk, consequently interfering with the growth factor signaling downstream of Ras (24–26). We presume that CI-1040 therefore reduces gene over-expression when an abnormality is present in the MEK pathway leading to increased cell growth and tumor production. Pre-clinical data from various animal models has indicated significant tumor growth inhibition (27). CI-1040 recently underwent phase II clinical trials.

In vitro and *in vivo* biotransformation studies, which include enzyme and cell preparations from animals and humans, are initiated early in a drug candidate discovery program, and play an important role during the drug development process. A major goal of studying the biotransformation of a drug in both *in vitro* and *in vivo* models is to ensure toxicology studies expose animals to the same therapeutic agent and metabolites as those observed in humans. In this study, we compared the metabolism of CI-1040 using *in vitro* and *in vivo* models with metabolism observed in a human bile sample. Typically both rodent and non-rodent models are chosen for drug safety studies. In this study, the rat, and the cynomolgus were chosen. Human bile is of particular interest as it is rarely available for metabolite identification studies after administration of a test compound. In this study, 600 mls of human bile was analyzed for metabolites. This sample was obtained from a cancer patient receiving CI-1040 during an efficacy study against tumor growth.

MATERIALS AND METHODS

Chemicals

Unlabeled and [^{14}C] labeled CI-1040 was synthesized at Pfizer, Inc., Global Research and Development (Ann Arbor, MI, USA). The [^{14}C]CI-1040 had radiochemical purity greater than 99.3% and a chemical purity greater than 99.7%. The chemical purity of all compounds was 99.5% or greater.

CI-1040 Cross-Species Microsomal Incubations

Pooled liver microsomes (20 mg/ml protein concentration) from Wistar rats and cynomolgus monkeys were ob-

[1] Department of Discovery Technologies, Pfizer Inc, Global Research and Development, Ann Arbor, Michigan, USA.
[2] Department of Clinical R&D, Pfizer Inc, Global Research and Development, Ann Arbor, Michigan, USA.
[3] Department of Otolaryngology, Queen Elizabeth Hospital, Adelaide, SA, Australia.
[4] To whom correspondence should be addressed. (e-mail: paul.wabnitz@pfizer.com)

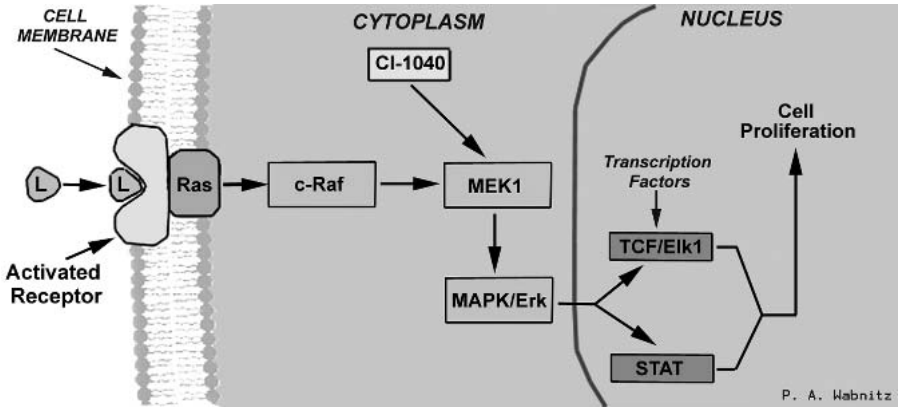

Fig. 1. CI-1040 (MEK 1 inhibitor) blocks the MAP Kinase cascade by prohibiting activation of MEK1. L = ligand; Ras = Prot-oncogene for Ras protein expression; c-Raf = cysteine rich MEK signaling protein; MEK1 = MAP-Erk kinase; MAPK = mitogen-activated protein kinase; Erk = extracellular signal-regulated kinase; TCF = T-cell factor; Elk1 = Ets domain protein; STAT = signal transducer and activator.

tained from Xenotech, LLC (Kansas City, KS). Pooled human liver microsomes (1 mg/ml protein) were obtained from Gentest Labs (Woburn, MA). [^{14}C]CI-1040 (20.9 μM, 10 μg/ml in acetonitrile) was incubated in duplicate with liver microsomal preparations from all species (0.5 mg/ml protein), containing NADPH (1 mM) in potassium phosphate buffer (50 mM, pH 7.4). Incubations were performed at 37°C. The samples were pre-incubated for 3 min to allow for temperature equilibration. Reactions were initiated with the addition of [^{14}C] CI-1040. Aliquots (0.250 ml) were removed from each incubate at 0, 10, 20, 30, 60, and 90 min. Control incubations with boiled human liver microsomes and incubations without NADPH were performed, which resulted in the absence of metabolites. Aliquots (0.25 ml) were removed at 0 and 60 min. All samples were immediately quenched with cold acetonitrile and stored at -80°C until analysis. On analysis, aliquots were thawed, centrifuged and the supernatant removed. The pellet was washed with acetonitrile (1 ml) and the combined supernatants evaporated to near dryness under nitrogen. The resulting residue was reconstituted in mobile phase and profiled. Characterization of the metabolites was achieved by LC/MS in combination with LC-MS/MS.

CI-1040 Hepatocyte Incubations

Cynomolgus monkey hepatocytes were obtained from Cedra Corp. (Austin, TX). Cryopreserved human hepatocytes (from a 65-year-old female Caucasian donor GB, lot 103) were procured from *in vitro* Technologies (Baltimore, MD). Human hepatocytes in Vidacyte gel (from a 62-year-old Hispanic female donor) were obtained from the International Institute for the Advancement of Medicine (IIAM) (Edison, NJ). Cells were extracted according to the specifications of the vendor. Both donors were HIV- and hepatitis B-free. Isolated rat hepatocytes in Vidacyte-2 gel (shipping medium) were received on ice. Vidacyte-2 gel was liquefied in a 37°C water bath for approximately 20 min. All hepatocyte preparations were centrifuged at 50 rpm for 5 min. The supernatant was discarded and the resulting material resuspended in William's E media on ice. A sample of the resuspended hepatocytes was treated with Trypan blue to count the initial number of cells. The initial viability of the isolated hepatocytes was assessed by Trypan Blue exclusion (87–98%). [^{14}C] CI-1040 (20.7 μM, 10 μg/ml in acetonitrile) was incubated in duplicate with rat, monkey and human hepatocyte suspensions in William's E media pH 7.4. Incubations were performed at 37°C in a shaking water bath. Samples were pre-incubated for 3 min to allow for temperature equilibration. Reactions were initiated with the addition of [^{14}C]CI-1040. Aliquots (0.5 ml) were removed from each incubate at 0, 10, 20, 30, 45, 60, 90, 120, and 180 min. All samples were immediately quenched with cold acetonitrile (5 ml) and stored at -80°C until analysis by HPLC-RAM. The samples were then profiled and the metabolites characterized by LC/MS and LC/MS/MS.

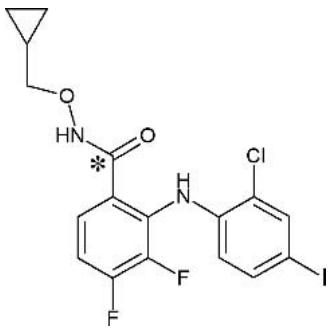

Fig. 2. Chemical structure of [^{14}C]CI-1040. *Denotes the metabolically stable position of the radiolabel.

CI-1040 Rat Mass Balance Study

Eight intact (Groups 1 and 3, four rats per group) and 4 bile duct-cannulated (Group 2; BDC) male Wistar rats were given a single 50 mg/kg oral dose of [^{14}C]CI-1040. Rats from Group 2 were lightly anesthetized (Isoflurane) 3 days before dose administration.. During the study, animals in groups 1 and 2 were housed in individual Nalgene metabolism cages designed for the separation and collection of urine, bile and feces. Urine and feces were collected from each animal predose and at 0–8, 8–24, 24–48, 48–72, 72–96, 96–120, and 120–144 h post dose. Additionally, in BDC rats (group 2), bile was collected at 0–2, 2–4, 4–6, 6–8, 8–24, 24–48, 48–72, 72–96, 96–120, and 120–144 h post dose. Group 3 were housed in

individual stainless steel wire-mesh cages and blood was collected at 2, 6, 8, and 24 h post-dose. Plasma (0.1 ml) harvested from the blood was treated twice with acetone in acetonitrile (3.0 ml/5%). The supernatant was evaporated to dryness, reconstituted in 0.5 ml diluent (50 mM ammonium formate adjusted to pH 3.7 with formic acid) and then centrifuged before profiling. The extraction recovery for 2-, 6-, 8-, and 24-h plasma was 84%, 71%, 84%, and 68%, respectively.

Urine (2.0 ml) from the 0- to 8- and 8- to 24-h collection intervals were lyophilized, reconstituted in 0.5 ml diluent, then centrifuged before profiling. The recovery of radioactivity from a representative 0- to 8-h sample was 92%.

Bile was centrifuged before profiling. Feces samples (0.5 ml) from intact and bile duct-cannulated (BDC) rats were treated twice with acetonitrile (3 ml). The supernatant was evaporated to dryness, reconstituted in 0.5 ml diluent (50 mM ammonium formate adjusted to pH 3.7 with formic acid), and then centrifuged before profiling. The extraction recoveries were greater than 80%. All samples were stored at -80°C until analysis. The samples were then profiled by HPLC-RAM, and the metabolites characterized by mass spectrometry.

CI-1040 Monkey Mass Balance Study

Three intact male cynomolgus monkeys (Phase I) were administered a single 50 mg/kg oral dose of [^{14}C]CI-1040 via gavage. Urine and feces were collected through 120 h post-dose at specified time intervals, and stored at -20°C until radio-analysis. Following the conclusion of Phase I, the animals then underwent surgery for bile duct cannulation (Phase II). Dosing and urine/feces/blood collections were similar to that described for Phase 1. In addition, bile was collected via the implanted cannula into plastic containers surrounded by wet ice at 0–2, 2–4, 4–6, 6–8, 8–24, 24–48, 48–72, 72–96, and 96–120 h intervals postdose. The plasma (0.1 ml) from the blood collection was treated twice with acetonitrile (3 ml). The supernatant was evaporated to dryness, reconstituted in 0.5 ml diluent (50:50, 50 mM ammonium formate at pH 3.7 with formic acid/acetonitrile), and then centrifuged before profiling. The extraction recovery was not determined due to insufficient levels of radioactivity.

Urine (2.0 ml) from the collection intervals was lyophilized, reconstituted in diluent (0.5ml), then centrifuged before profiling. Urine was collected from animals in plastic containers surrounded by wet ice at 0–8, 8–24, 24–48, 48–72, 72–96, and 96–120 h post-dose intervals. Feces were collected at room temperature and transferred into plastic containers at 0–24, 24–48, 48–72, 72–96, and 96–120 h post-dose intervals. Feces aliquots were then treated twice with 3.0 ml of 5% acetone in acetonitrile. The supernatant was evaporated to dryness, reconstituted in 0.5 ml diluent (50 mM ammonium formate adjusted to pH 3.7 with formic acid), and then centrifuged before profiling. The mean extraction recovery was 94%. All samples were stored at –80°C until analysis. The samples were then profiled by HPLC-RAM, and the metabolites characterized by mass spectrometry.

CI-1040 Administration to Man

Unlabeled CI-1040 was administered orally in capsules (100 mg QD for 15 days to a white Caucasian male (65 years old, 62.2 kg) diagnosed with advanced colon cancer. Bile was obtained using a T-tube via bile duct cannulation during a surgical procedure in relation to a separate medical issue. The bile was collected over a period of 12–14 h, immediately following an oral dose (100 mg) of the unlabeled CI-1040. Blood samples for this investigation were collected intravenously on day 15 at 2, 6, and 12-h time-points after drug dosage. The plasma was separated from the red blood cells by centrifugation (3,000 rpm for 5 min). Resulting plasma (0.1 ml) from the blood collection was treated twice with 3.0 ml of 3% water in acetonitrile. Supernatant was then evaporated to dryness, reconstituted in diluent (0.5 ml, 50 mM ammonium formate adjusted to pH 3.7 with formic acid), and then centrifuged before profiling. This clinical study was conducted in compliance with the revised Declaration of Helsinki (1989) and was approved by a local ethical review committee at the Harper Hospital, Wayne State Medical Center, Michigan, United States.

Radioactivity Determination and Profiling

Metabolite profiling was achieved by HPLC (Series 200, Perkin Elmer) with an in-line radioactivity flow detector (β-RAM, IN/US). The samples under investigation were measured for radioactivity by liquid scintillation counting (Model TR2500, Packard Instruments, Boston, MA). Sample aliquots were directly injected and the radioactive peaks were resolved using a Zorbax RX-C8 reversed-phase HPLC column (4.6 mm ID × 250 mm). Column effluent was mixed with Ultima-Flo M scintillant (Packard) at a rate of 3.0 ml/min. The mobile phase, which consisted of ammonium formate (50 mM, pH adjusted to 3.7 with formic acid, Solvent A) and acetonitrile (Solvent B) was maintained at a constant flow rate (1 ml/min). A linear gradient with initial conditions of 95% solvent A and 5% solvent B was run for 60 min to 35% solvent A and 65% solvent B. The gradient was then held for an additional 10 min at 35% solvent A before the column was equilibrated for 10 min to initial conditions. Representative samples were then analyzed by mass spectrometry.

Metabolite Identification

Metabolite characterization was performed by the comparison of retention times on a gradient HPLC system with reference material. In addition, mass spectral analysis was performed to characterize the identity of all major radioactive peaks. Samples were directly injected onto the HPLC column through an autosampler (HP 1100 G1313A, Agilent Technologies, Wilmington, DE). Chromatographic separation was performed using a Luna C_{18}-A column (4.6 × 150 mm, 5-μm particle size, Phenomenex, Torrance, CA) together with a SecurityGuard column (4.6 mm C_{18}-A, 5-μm particle size, Phenomenex.). Gradient conditions were the same as described above. All LC-MS and LC-MS/MS experiments were performed using a Quadrupole ion trap mass spectrometer (ThermoFinnigan, San Jose, CA) coupled with a HPLC (HP 1100 Binary Pump [G1312A] and UV detection (HP 1100 Dual Wavelength G1365A, 280 nm, Agilent Technologies). Sample introduction into the mass spectrometer was achieved by using electrospray ionization (ESI) in the negative mode. LC-MS spectra were acquired by scanning over 100–1300 amu. Collision activation mass spectral data in negative mode were obtained using collision energies ranging from 30% to

35%. Electrospray conditions were as follows: source voltage 4.5 kV, capillary temperature 300°C, capillary voltage 11 V, Lens voltage –25 V. Mass spectra were obtained with the automatic gain control on, with a maximum ion time of 400 ms, and using 3 microscans per scan, averaging over approximately 20 scans. For both LC-MS and LC-MS/MS experiments, a Windows NT based computer system was used for instrument control, data acquisition and data processing. Data acquisition, analysis and processing were achieved by using Xcalibur software (Version 1.0, ThermoQuest, San Jose, CA). The N-glucuronide metabolite (M7) was distinguished from the O-glucuronide (M8) using LC/MS/MS (28). The o-glucuronide metabolite displayed a characteristic loss of a hydroxy-glucuronide (192 Da.), which was not observed by the fragmentation pattern of the N-glucuronide metabolite. Additionally, the N-glucuronide metabolite eluted earlier than the O-glucuronide metabolite, which was expected.

RESULTS

CI-1040 Metabolites from Liver Microsomal Incubates

Gradient HPLC profiling and mass spectral analysis of the 90-min microsomal incubations revealed several major components (Table I). Qualitatively, the human liver microsomal metabolic profile appeared similar to that obtained from the rat, and monkey liver microsomal profiles. The major radioactive component detected in all species was the parent drug CI-1040, which accounted for 27.9–48.5% of the total radioactivity. Structural elucidation of this component, using LC/MS/MS experiments of the deprotonated molecular ion of *m/z* 477, gave rise to ions of *m/z* 459, 441, 405 and 370 (Fig. 3). This fragmentation information further indicated the identity of this major component as being the parent drug CI-1040. The major metabolite characterized in all microsomal species was characterized as 2-(2-chloro-4-iodo-phenylamino)-3,4-difluoro-benzoic acid (M_6) and represented 18.6–29.2% of the total radioactivity. Additionally, other identified components in the microsomal samples were characterized as monohydroxy 2-(2-chloro-4-iodo-phenylamino)-3,4-difluoro-benzoic acid (M_1), monohydroxy 2-(2-chloro-4-iodo-phenylamino)-3,4-difluoro-benzamide (M_2), monohydroxy 2-(2-chloro-4-iodo-phenylamino)-3,4-difluoro-benzamide (M_3), monohydroxy CI-1040 (M_4) and 2-(2-chloro-4-iodo-phenylamino)-3,4-difluoro-benzamide (M_5). M_1 was not detected in the rat. The structures of all microsomal metabolites were confirmed by LC/MS/MS experiments.

CI-1040 Metabolites from Hepatocyte Incubates

Two major radioactive components were found present in all hepatocyte species and were identified as the parent drug CI-1040 (7.9–32.8% of the total radioactivity in each species) and 2-(2-chloro-4-iodo-phenylamino)-3,4-difluoro-benzoic acid (M_6, 23.2–31.8% of the total radioactivity in each species). The percent radiochromatogram that each radioactive component represents from the *in vitro* studies are summarized in Table I. Qualitatively, the human hepatocyte metabolic profile appeared most similar to that obtained from the monkey hepatocyte profiles. Additional metabolites characterized in the hepatocyte incubations compared to those observed in the microsomal incubations, included monohydroxy CI-1040 (M_4), 2-(2-chloro-4-iodo-phenylamino)-3,4-difluoro-benzamide (M_5), 2-(2-chloro-4-iodo-phenylamino)-3,4-difluoro-benzoic acid (M_6), N-glucuronide conjugate of monohydroxy M_6 (M_7), O-glucuronide conjugate of monohydroxy M_6 (M_8), N-glucuronide conjugate of defluoro-monohydroxy M_6 (M_9), O-glucuronide conjugate of monohydroxy CI-1040 (M_{10}) and N-glucuronide conjugate of CI-1040 (M_{11}). The structures of all metabolites isolated from the hepatocytes were further confirmed by LC/MS/MS experiments. A compilation of all metabolites identified from both the microsomal and hepatocyte incubations is represented by the metabolic scheme shown in Fig. 4.

Rat Mass Balance CI-1040 Metabolites

A compilation of all metabolites identified from both the rat and monkey mass balance experiments is represented by the proposed metabolic scheme shown in Fig. 4. In intact rats (Group 1), the total mean recovery of radioactivity in urine, feces, cage rinse, cage wash and cage wipes was 94.5%. Feces and urine accounted for a mean of 91.8% and 2.58% of the total administered radioactivity, respectively. The radioactivity was excreted rapidly with at least 78% of the radioactivity excreted in the feces and urine within 24 h postdose. Since the amount of radioactivity in 0- to 8- and 8- to 24-h urine collections was too low for direct injection, each sample was lyophilized before profiling. Despite concentrating these

Table I. Radioactive Components (Percent Chromatogram) from *in Vitro* Incubates

Radioactive components (% chromatogram) in 90-min microsomal incubates							
Species	M_1	M_2	M_3	M_4	M_5	M_6	CI-1040
Rat	ND	2.01	6.05	6.12	7.14	28.31	48.54
Monkey	7.72	1.75	15.71	10.82	6.52	18.55	27.92
Human	2.11	1.62	10.52	10.63	6.81	29.24	33.34

Radioactive components (% chromatogram) in 180-min hepatocyte incubates									
Species	M_4	M_5	M_6	M_7	M_8	M_9	M_{10}	M_{11}	CI-1040
Rat	14.30	15.22	31.71	ND	11.13	11.24	ND	ND	32.84
Monkey	5.75	5.82	23.23	6.71	6.82	10.68	6.91	9.92	7.92
Human	9.82	10.10	31.82	ND	5.21	7.81	4.22	8.43	12.26

ND = not detected.

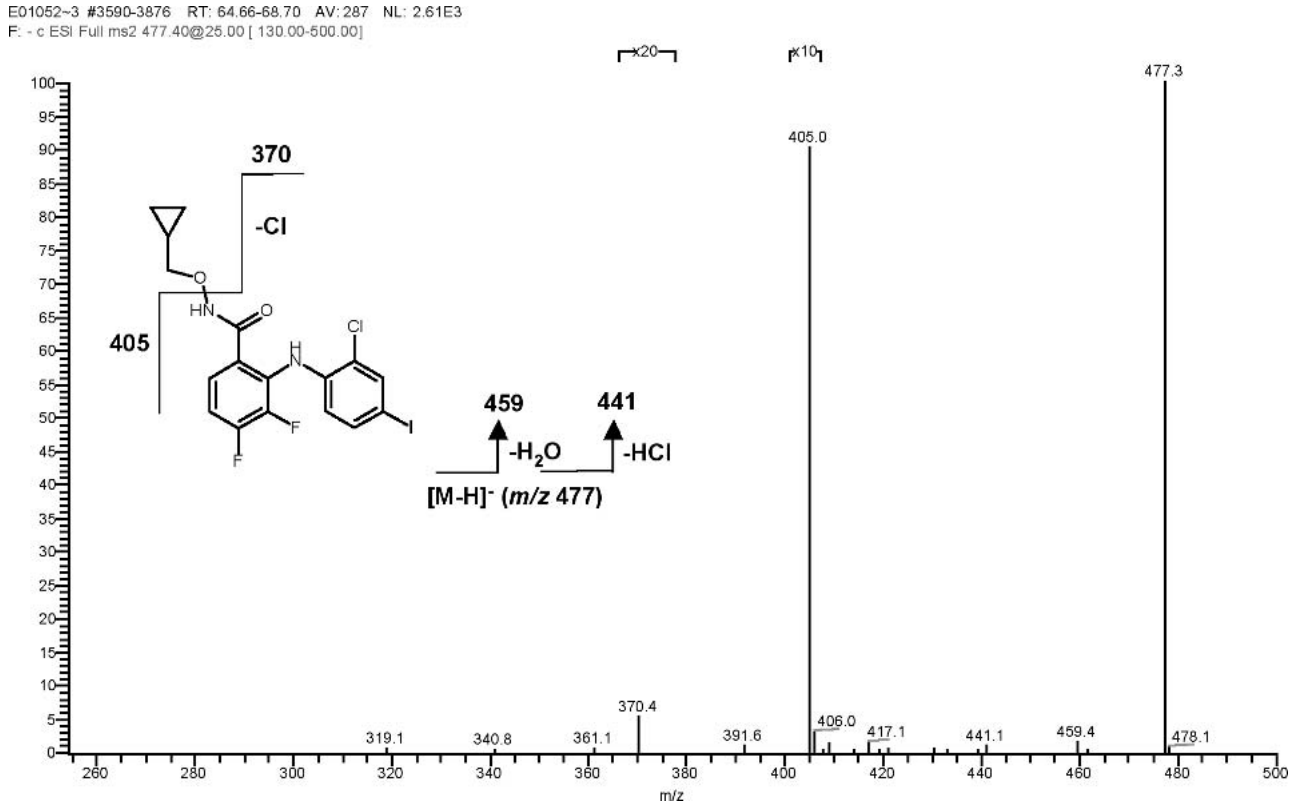

Fig. 3. LC-MS/MS spectrum of the $[M-H]^-$ ion of CI-1040 (*m/z* 477).

samples 4-fold, the radioactivity was too low to detect metabolites.

In BDC rats (Group 2), the total mean recovery of radioactivity in urine, bile, feces, cage rinse, cage wash, cage wipes, jacket rinse and bile cannulas was 97.6%. Feces, bile, and urine accounted for a mean of 55.2%, 41.4%, and 0.96% of the total administered radioactivity, respectively. The radioactivity was excreted rapidly with 94.1% of the radioactivity excreted in the feces, bile, and urine within 24 h post dose. Urine samples were not profiled due to insufficient levels of radioactivity.

A summary of the components revealed by HPLC profiling and mass spectral analysis of the rat mass balance samples is listed in Table II. The major radioactive peak in extracted plasma from 2, 6 and 8-h blood collections was characterized as 2-(2-chloro-4-iodo-phenylamino)-3,4-difluoro-benzoic acid (M_6). Unchanged CI-1040 was the second most abundant radioactive component in the plasma, with a much lesser peak characterized as the O-glucuronide conjugate of monohydroxy M_6 (M_8). The most abundant radioactive component excreted in bile was CI-1040, accounting for approximately 47.3% of the 94.1% of dose excreted during the first 24 h post dose. Seven additional radioactive components were detected in the bile, with the most abundant metabolite being characterized as an N-glucuronide conjugate of CI-1040 (M_{11}). This metabolite represented 9.01% of the dose excreted in bile during the first 24-hours post-dose. Radioactive analysis from BDC male rat feces extracts (8 to 24 h) identified CI-1040 as the major radioactive component, which was responsible for 44% of the radioactivity excreted in feces during the first 24 h post dose. Five additional metabolic components, identified as M_4, M_5, M_6, M_{13}, and M_{14}, were also detected as being present in the fecal extract. The structures of all metabolites isolated from the rat samples were further confirmed by LC/MS/MS experiments

Monkey Mass Balance CI-1040 Metabolites

In intact monkeys (Phase I), the total mean recovery of radioactivity in urine, feces, cage debris, cage wash and cage wipes was 85.1%. Feces and urine accounted for a mean of 84.2% and 0.52% of the total administered radioactivity, respectively. By 72 h post dose, 79.8% of the radioactivity was recovered in feces.

In BDC monkeys (Phase 2), the total mean recovery of radioactivity in urine, bile, feces, cage wash and cage wipes was 90.7%. Feces, bile, and urine accounted for a mean of 81.7%, 8.0%, and 0.27% of the total administered radioactivity, respectively. By 72 h post dose, 78.9% of the radioactivity was recovered in the feces and 7.7% was recovered in the bile.

Urine samples were not profiled due to insufficient levels of radioactivity. The major radioactive peak in extracted plasma (Phase II) from 2- and 8-h blood collections were characterized as 2-(2-chloro-4-iodo-phenylamino)-3,4-difluoro-benzoic acid (M_6). Unchanged CI-1040 was the second most abundant radioactive component in the plasma, with three additional metabolic components also being detected in lesser quantities. Six of the eight radioactive components detected in monkey bile were previously characterized in the rat mass balance samples. However, the parent drug CI-1040, which was a major component from the rat bile, was not detected in the monkey bile sample. Radioactive analysis from male monkey (Phase II) feces extracts (0 to 72-h) identified CI-1040 as the major radioactive component,

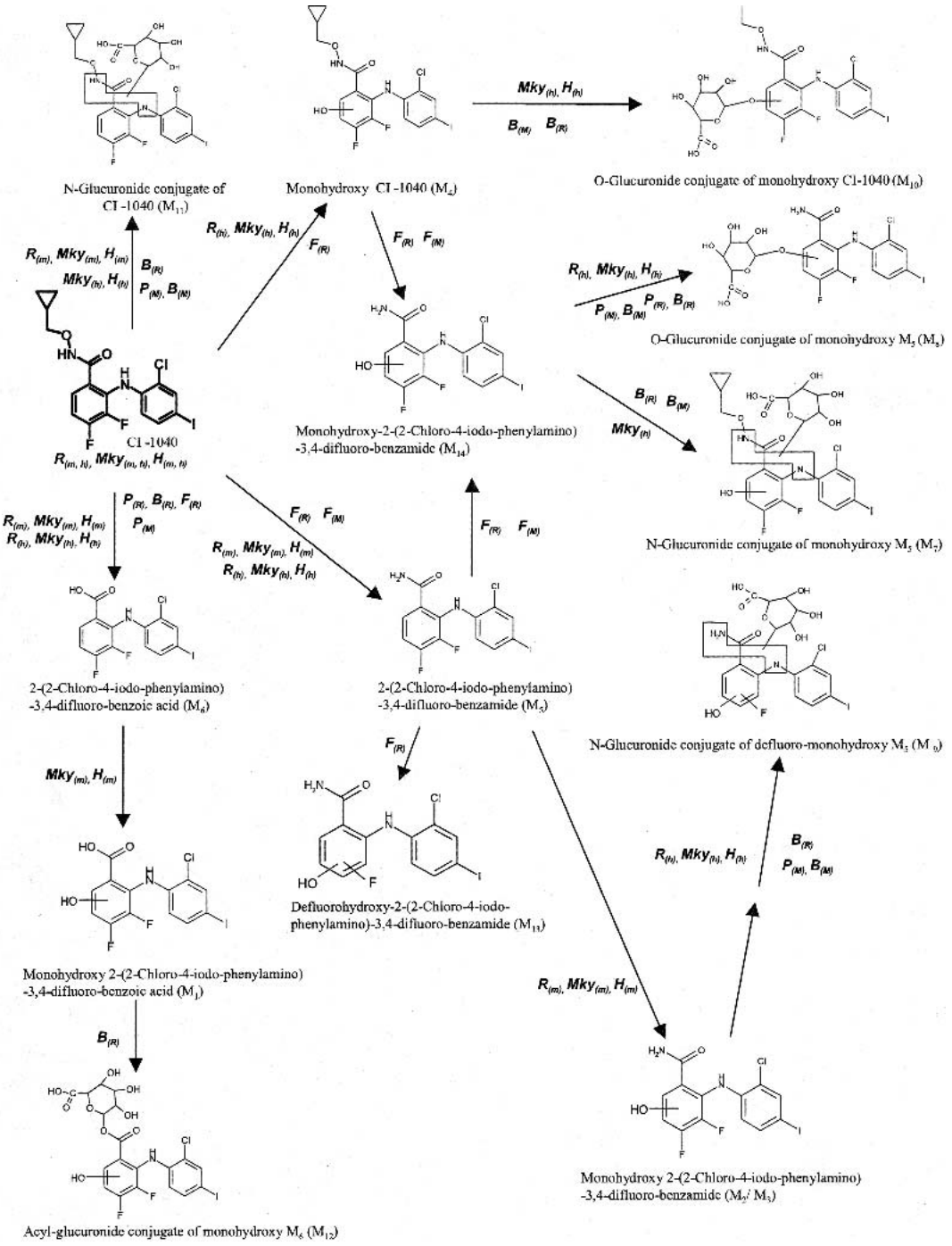

Fig. 4. Biotransformation pathway of [^{14}C]CI-1040 in rat, monkey and human microsomes, hepatocytes, and rat and monkey plasma, bile, and fecal extracts. $R_{(m)}$ = rat liver microsomes; $Mky_{(m)}$ = monkey liver microsomes; $H_{(m)}$ = human liver microsomes; $R_{(h)}$ = rat liver hepatocytes; $Mky_{(h)}$ = monkey liver hepatocytes; $H_{(h)}$ = human liver hepatocytes; $P_{(R)}$ = rat plasma; $B_{(R)}$ = rat bile; $F_{(R)}$ = rat feces; $P_{(M)}$ = monkey plasma; $B_{(M)}$ = monkey bile; $F_{(F)}$ = monkey feces.

which was responsible for 21.4% of the radioactivity excreted in feces during the first 24 h post dose. Two additional metabolic components were also detected, which were identified as the M_5 and M_{14} metabolites. The percent radiochromatogram that each radioactive component represents from the in-vivo studies are summarized in Table II. The structures of all metabolites isolated from the monkey samples were confirmed by LC/MS/MS experiments.

CI-1040 Metabolites from Human Plasma and Bile

Human clinical samples were collected for analysis following an oral dose (100 mg) of unlabeled CI-1040. The subject was a 65-year old male (62 kg) diagnosed with advanced colon cancer. The dose of CI-1040 was well tolerated by the subject. Drug related components present in the clinical samples were identified and characterized solely by LC/MS

Table II. Radioactive Components (Percent Chromatogram) from Rat and Monkey *in Vivo* Samples

Radioactive components (% chromatogram) in rat plasma (Group 3 male rats, 50 mg/kg [^{14}C]CI-1040 oral dose)			
Time (h)	M_6	M_8	CI-1040
2	82.50	3.40	6.72
6	84.80	9.01	1.79
8	70.71	2.76	18.62

Radioactive components (% chromatogram) in rat bile (Group 2 male rats, 50 mg/kg [^{14}C]CI-1040 oral dose)								
Time (h)	M_6	M_7	M_8	M_9	M_{10}	M_{11}	M_{12}	CI-1040
0–4	0.18	1.37	1.37	0.79	0.29	8.29	0.42	43.0
4–8	0.57	3.06	3.06	1.29	0.39	7.39	1.62	51.0
8–24	0.60	3.11	3.11	1.28	0.13	11.35	1.47	47.9

Radioactive components (% chromatogram) in rat feces (Group 2 male rats, 50 mg/kg [^{14}C]CI-1040 oral dose)						
Time (h)	M_4	M_5	M_6	M_{13}	M_{14}	CI-1040
8–24	18.40	18.40	2.45	18.40	5.60	44.00
24–48	3.68	3.68	0.68	3.68	5.11	1.92

Radioactive components (% chromatogram) in monkey plasma (50 mg/kg [^{14}C]CI-1040 oral dose)					
Time (h)	M_6	M_8	M_9	M_{11}	CI-1040
2	79.68	4.50	3.38	6.74	7.63
8	84.55	6.78	ND	5.47	ND

Radioactive components (% chromatogram) in Phase II monkey bile (50 mg/kg [^{14}C]CI-1040 oral dose)						
Time (h)	M_7	M_8	M_9	M_{10}	M_{11}	CI-1040
2–4	—	0.11	0.12	0.03	0.14	ND
4–6	0.01	0.09	0.10	0.02	0.10	ND
6–8	0.01	0.06	0.01	ND	0.09	ND
8–24	0.08	0.19	0.10	0.01	0.37	ND

Radioactive components (% chromatogram) in Phase II monkey feces (50 mg/kg [^{14}C]CI-1040 oral dose)			
Time (h)	M_5	M_{14}	CI-1040
0–24	0.13	—	21.40
24–48	0.79	0.03	62.30
48–72	0.16	0.02	2.98

ND = not detected.

and LC/MS/MS experiments. Characterization of the human plasma metabolites by mass spectrometry identified the presence of the parent drug CI-1040, 2-(2-chloro-4-iodo-phenylamino)-3,4-difluoro-benzoic acid (M_6), N-glucuronide conjugate of monohydroxy M_6 (M_7), O-glucuronide conjugate of monohydroxy M_6 (M_8), and the N-glucuronide conjugate of CI-1040 (M_{11}). LC/MS/MS experiments confirmed the structure of the M_6 metabolite as the benzoic acid. The structures of all additional metabolic products observed were also confirmed by LC/MS/MS. Mass spectrometry characterization of the human bile identified the presence of the parent drug CI-1040, 2-(2-chloro-4-iodo-phenylamino)-3,4-difluoro-benzoic acid (M_6), N-glucuronide conjugate of monohydroxy M_6 (M_7), O-glucuronide conjugate of monohydroxy M_6 (M_8), N-glucuronide conjugate of CI-1040 (M_{11}) and the acyl-glucuronide conjugate of monohydroxy M_6 (M_{12}), which was not detected in the clinical plasma samples investigated. The respective extracted ion chromatograms (XIC) of all metabolic products observed by mass spectrometry in the bile are displayed in Fig. 5. LC/MS/MS experiments confirmed the structure of all metabolic products observed in the bile. A representation of the fragmentation pattern obtained by LC/MS/MS of M_8 is demonstrated in Fig. 6. A compilation of the metabolites identified from the human plasma and bile samples is summarized in Table III. Cross species comparison of all metabolic products detected from the *in vitro* and *in vivo* samples can now be established with the human clinical products.

A summary of this comparison for all metabolites across species is presented in Table III.

DISCUSSION

CI-1040, a potent MEK inhibitor with potential for therapeutic benefit against cancer and inflammatory diseases, was observed to undergo extensive oxidative metabolism and

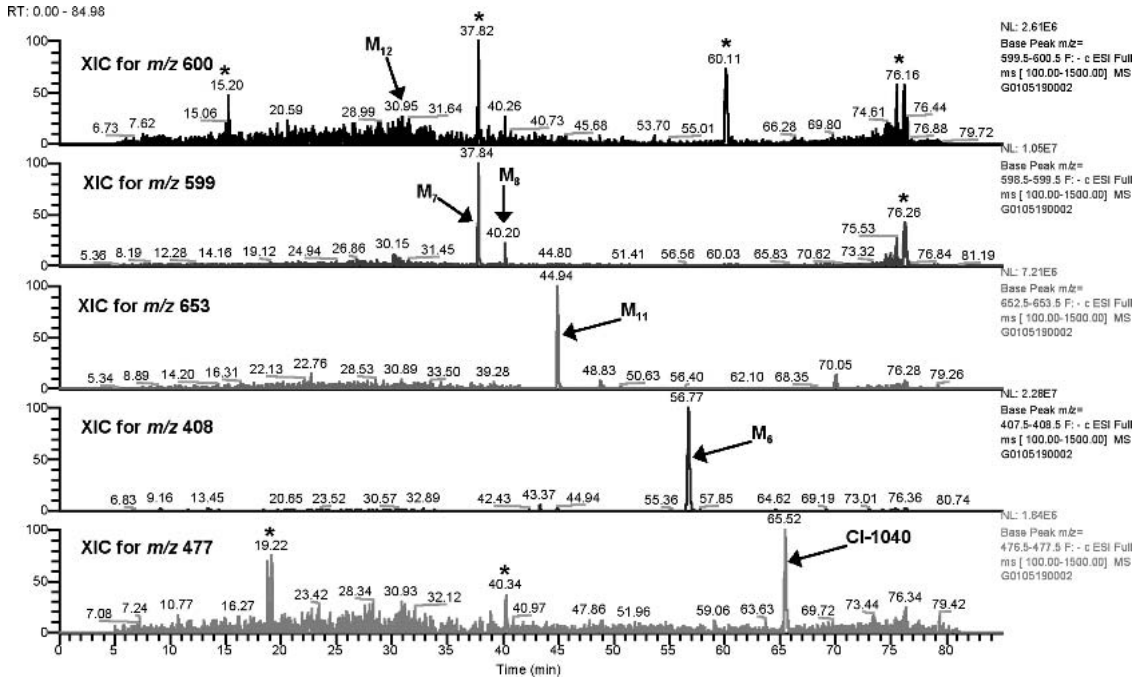

Fig. 5. Extracted ion chromatograms (XIC) of CI-1040 metabolism products derived from human bile (0–14 h post-dose). *Denotes artifact peak.

glucuronidation in rats, monkeys, and a human cancer patient. CI-1040 is extensively excreted in the feces in all species studied. This is most likely due to the low solubility of CI-1040 that somewhat limits the absorption of the compound (23). Many of the hydroxylated metabolites were subsequently glucuronidated and excreted predominantly in bile and feces. Metabolic profiles involving administration of CI-1040 in microsomes and hepatocytes were generally shown to be qualitatively similar across species. In total, fourteen metabolites were characterized, and the profile from the *in vitro* and animal models in combination was able to successfully predict the metabolites observed in human bile and/or plasma.

2-(2-chloro-4-iodo-phenylamino)-3,4-difluoro-benzoic acid (M_6) was the major metabolite generated *in vitro* for all species (rat, monkey and human). The mechanism of amide cleavage to form M_6 has not been determined, but there is evidence for both cytochrome P450 (CYP) and non-CYP catalysis (29,30). Reaction phenotyping data using recombinant

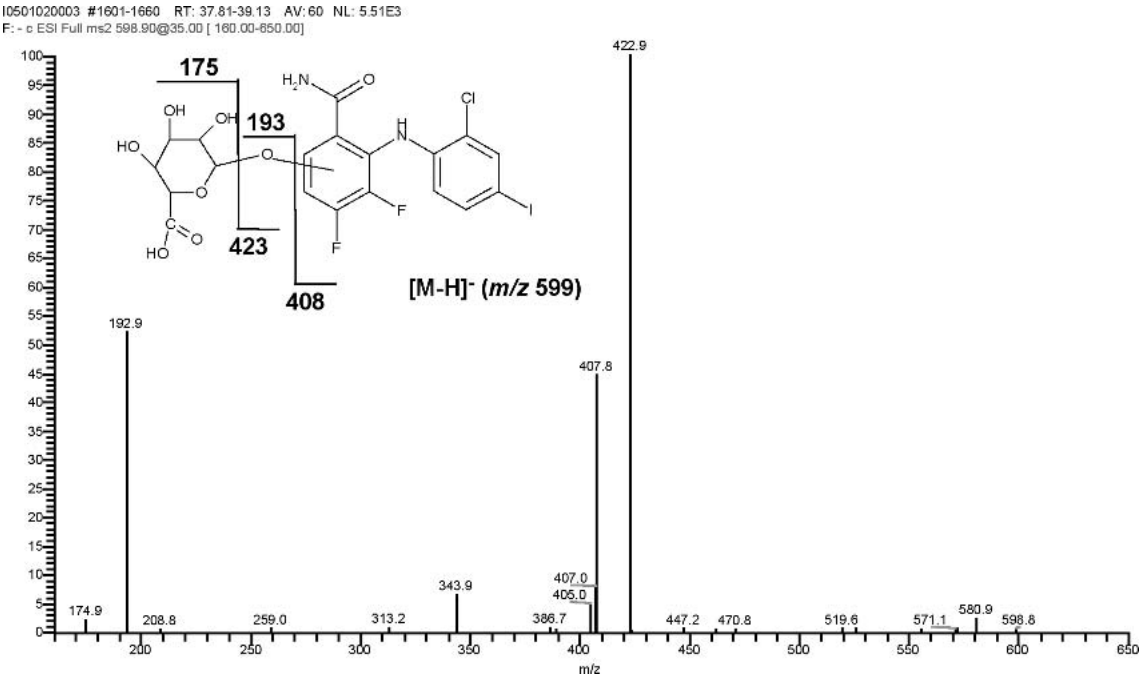

Fig. 6. LC-MS/MS spectrum of the $[M-H]^-$ ion of M_8 [O-Glucuronide conjugate of monohydroxy M_6] (*m/z* 599).

Table III. Comparison Summary of All Metabolites Detected from Rat, Monkey, and Human Samples

Sample	M_1	M_2	M_3	M_4	M_5	M_6	M_7	M_8	M_9	M_{10}	M_{11}	M_{12}	M_{13}	M_{14}	CI-1040
Microsomes															
Rat	ND	√	√	√	√	√	ND	ND	ND	ND	ND	ND	ND	ND	√
Monkey	√	√	√	√	√	√	ND	ND	ND	ND	ND	ND	ND	ND	√
Human	√	√	√	√	√	√	ND	ND	ND	ND	ND	ND	ND	ND	√
Hepatocytes															
Rat	ND	ND	ND	√	√	√	ND	√	√	ND	ND	ND	ND	ND	√
Money	ND	ND	ND	√	√	√	√	√	√	√	√	ND	ND	ND	√
Human	ND	ND	ND	√	√	√	ND	√	√	√	√	ND	ND	ND	√
Rat mass balance															
Plasma	ND	ND	ND	ND	ND	√	ND	√	ND	ND	ND	ND	ND	ND	√
Bile	ND	ND	ND	ND	ND	√	√	√	√	√	√	√	ND	ND	√
Feces	ND	ND	ND	√	√	√	ND	ND	ND	ND	ND	ND	√	√	√
Monkey mass balance															
Plasma	ND	ND	ND	ND	ND	√	ND	√	√	ND	√	ND	ND	ND	√
Bile	ND	ND	ND	ND	ND	ND	√	√	√	√	√	ND	ND	ND	ND
Feces	ND	ND	ND	ND	√	ND	ND	ND	ND	ND	ND	ND	ND	√	√
Human															
Plasma	ND	ND	ND	ND	ND	√	√	√	ND	ND	√	ND	ND	ND	√
Bile	ND	ND	ND	ND	ND	√	√	√	ND	ND	√	√	ND	ND	√

ND = not detected.
√ = metabolite detected and characterized.

human CYP enzymes indicates that CYP1A1, CYP1A2 and CYP2C19 catalyze this biotransformation (23). In addition, since M_6 was formed in the absence (as well as the presence) of the CYP/FMO cofactor NADPH with human liver microsomes, a non-P450/non-FMO amidase also appears to contribute. The extent of the formation of M_6 was almost identical in both the NADPH-dependent and non-NADPH-dependent conditions. The absence of metabolite formation after incubation with boiled microsomes indicates that the presence of active enzyme(s) is (are) necessary for the reaction to proceed. Hydroxylated metabolites (M_1, M_2, M_3) were primarily detected only in the liver microsomes, and not in the liver hepatocytes of all species investigated. This can be explained by the observation of the predominant presence of glucuronide conjugates of monohydroxy metabolites in the hepatocytes. This indicates that the hydroxy-metabolites were most likely totally converted to glucuronide metabolites most likely for elimination purposes. Consequently, increasing the overall hydrophilicity of a once hydrophobic compound.

The *in vivo* results showed marked differences in the relative abundance of metabolites between plasma, bile and feces. For example, M_6 was the major component in the rat plasma, whereas CI-1040 was the major component and M_{11} (CI-1040 N-glucuronide) the major metabolite in rat bile and feces. For cynomolgus monkeys, M_6 was undetected in the monkey bile and plasma, but was observed as the main constituent in the feces. As with the rat, M_{11} (CI-1040 N-glucuronide) was the most abundant phase II metabolite in both the monkey bile and plasma samples. For the human bile sample, the administration of unlabelled CI-1040 did not allow comparison of the relative abundance of each metabolite. However, as with the rat and monkey, CI-1040 underwent extensive oxidative metabolism, glucuronidation, and subsequent glucuronidation of the hydroxylated metabolites in a male cancer patient. It is interesting to note that the unchanged drug was not detected in the monkey bile, but was detected in the rat and human bile. This observation may be due to a species difference possibly involving a varying rate of turnover or an elimination route difference specific only for the monkey with the metabolism of this particular drug.

In the bile duct-cannulated rats, biliary excretion (~41%) and fecal extract (~55%) accounted for the majority of the [^{14}C] radiolabeled compound. Renal elimination of radioactivity for rat and monkey was minimal (<5% of dose). Analysis of urine from the cancer patient showed virtually no metabolites of CI-1040 to be present. As the metabolic profile from the human bile sample determined the presence of the parent drug CI-1040 and five additional metabolites, and no drug-related compounds were observed in the urine, it is suspected that most of the parent compound and metabolites would be excreted in the bile in humans.

In conclusion, the results obtained in this study demonstrate the utility of conducting investigations across species in order to gain complete coverage for successfully predicting human metabolites of new compounds in development. This was demonstrated in this investigation by the use of *in vitro* and *in vivo* models, human plasma and a rare clinical bile sample.

ACKNOWLEDGMENTS

The authors would like to thank Barbara Michniewicz for her contributions in obtaining the necessary rat and monkey *in vivo* data used in this publication. Additionally, we would like to acknowledge Andy Williams, Abdul Mutlib, Cho-Ming Loi, and Susan Hurst for their editorial assistance.

REFERENCES

1. M. Melameds. Lung cancer screening results in the National Cancer Institute New York Study. *Cancer Res.* **89**:2356–2362 (2000).

2. G. Brundtlan. Global Health Situation and Trends 1955-2025. Fifty Facts from The World Health Report, Wiley-Interscience, New York (1998).
3. J. Sebolt-Leopold, D. Dudley, R. Herrera, K. Van Becelaere, A. Wiland, R. Gowan, H. Tecle, S. Barrett, A. Bridges, S. Przybranowsk, W. Leopold, and L. A. Saltie. Blockade of the MAP kinase pathway suppresses growth of colon tumors *in vivo*. *Nat. Med.* **5**:810–816 (1999).
4. J. Sebolt-Leopold. Development of anticancer drugs targeting the MAP kinase pathway. *Oncog.* **19**:6594–6599 (2000).
5. L. A. Saltie. PD098059 Is a Specific Inhibitor of Mitogen-Activated Protein Kinase *in vitro* and *in vivo*. *Scientist* **11**:12 (1997).
6. L. Pang, T. Sawada, S. J. Decker, and A. R. Saltiel. Inhibition of MAP kinase kinase blocks the differentiation of PC-12 cells induced by nerve growth factor. *J. Biol. Chem.* **270**:13585–13588 (1995).
7. M. Cobb and E. Goldsmith. How MAP kinases are regulated. *J. Biol. Chem.* **270**:14843–14846 (1995).
8. T. Shih, M. Weeks, P. Gruss, R. Dhar, S. Oroszlan, and E. Scolnick. Identification of a precursor in the biosynthesis of the p21 transforming protein of harvey murine sarcoma Virus. *J. Virol.* **42**:253–261 (1982).
9. M. Streit, R. Schmidt, R. U. Hilgenfeld, E. Thiel, and E. D. Kreuser. Adhesion receptors in malignant transformation and dissemination of gastrointestinal tumors. *J. Mol. Med.* **74**:253–268 (1996).
10. S. Talapatra and C. Thompson. Growth factor signaling in cell survival: implications for cancer treatment. *J. Pharm. Exp. Ther* **298**:873–878 (2001).
11. C. Zheng and K. Guan. Properties of MEKs, the kinases that phosphorylate and activate the extracellular signal-regulated kinases. *J. Biol. Chem.* **268**:23933–23939 (1993).
12. Y. Yarden and M. Sliwkowski. Untangling the ErbB signaling network. *Nat. Med.* **2**:127–137 (2001).
13. P. Warne and P. Viciana. and J. Downward. Direct interaction of Ras and the amino-terminal region of Raf-1 in vitro. *Nat. Med.* **364**:352–355 (1993).
14. S. Tanimura, Y. Chatani, R. Hoshino, M. Sato, S. Watanabe, T. Kataoka, T. Nakamura, and M. Kohno. Activation of the 41/43 kDa mitogen-activated protein kinase signaling pathway is required for hepatocyte growth factor-induced cell scattering. *Oncog.* **17**:57–65 (1998).
15. C. Simon, J. Juarez, G. Nicolson, and D. Boyd. Effect of PD 098059, a specific inhibitor of mitogen-activated protein kinase, on urokinase expression and in vitro invasion. *Cancer Res.* **56**: 5369–5374 (1996).
16. A. Shiamura, B. Ballif, and S. Richards. and J. Blenis. Rsk1 mediates a MEK-MAP kinase cell survival signal. *Curr. Biol.* **10**: 127–135 (2000).
17. G. Pages, J. Milanini, D. E. Richard, E. Berra, E. Gothie, and F. Vinals. and J. Pouyssegur. Signaling angiogenesis via p42/p44 MAP kinase cascade. *Ann. N. Y. Acad. Sci.* **902**:187–200 (2000).
18. P. Kurada and K. White. Ras promotes cell survival in Drosophiila by down-regulating hid expression. *Cell* **95**:319–329 (1998).
19. J. Gibbs. Mechanism-based target identification and drug discovery in cancer research. *Science* **287**:1969–1973 (2000).
20. D. Robbins, E. Zhen, M. Cheng, S. Xu, D. Ebert, and M. Cobb. MAP kinases ERK1 and ERK2: Pleiotropic enzymes in a ubiquitous signaling network. *Adv. Cancer Res.* **63**:93–116 (1994).
21. K. Sikora. Developing a global strategy for cancer. *Eur. J. Cancer* **35**:1870–1877 (1999).
22. J. Bos. Ras oncogenes in human cancer: a review. *Cancer Res.* **49**:4682–4689 (1989).
23. D. Y. Mitchell, J. M. Reid, R. E. Parchment, M. B. Meyer, J. S. Leopold, R. Herrera, J. R. Piens, L. M. Bruzek, L. J. Hanson, K. Van Becelaere, T. Carlson, C. Packard, A. A. Adjei, and P. M. LoRusso. Pharmacokinetics (PK) and pharmacodynamics (PD) of the oral MEK inhibitor, CI-1040, following multiple dose administration to patients with advanced cancer. *Proc. Am. Soc. Clin. Oncol.* **21**:81 (2002).
24. R. Seger and E. Krebs. The MAPK signaling cascade. *FASEB* **9**:726–735 (1995).
25. R. Seger, N. Ahn, J. Posada, E. Munar, A. Jensen, J. Cooper, M. Cobb, and E. Krebs. Purification and characterization of mitogen-activated protein kinase activator(s) from epidermal growth factor-stimulated A431 cells. *J. Biol. Chem.* **267**:14373–14381 (1992).
26. C. Tournier, C. Dong, T. Turner, S. Jones, R. Flavell, and R. Davis. MKK7 is an essential component of the JNK signal transduction pathway activated by proinflammatory cytokines. *Genes Dev.* **15**:1419–1426 (2001).
27. J. S. Sebolt-Leopold. Development of anticancer drugs targeting the MAP kinase pathway. *Oncog.* **19**:6594–6599 (2000).
28. J. Uusitalo, J. Jalonen, and O. Pelkonen. Identification of N+- and O-glucuronides of finrozole by LC/TOF, LC/MS/MS and LC/PB/MS. *Adv. Mass Spec.* **15**:693–694 (2001).
29. T. C. Sarich and T. Adams. P Stephen, P. Petricca, G. Giorgio, and J.M. Wright. Inhibition of isoniazid-induced hepatotoxicity in rabbits by pretreatment with an amidase inhibitor. *J. Pharm. Exp. Ther* **289**:695–702 (1999).
30. Y. Ono, X. Wu, A. Noda, H. Noda, and T. Yoshitani. Participation of P450-dependent oxidation of isoniazid in isonicotinic acid formation in rat liver. *Biol. Pharm. Bull.* **21**:421–425 (1998).